EurJIC European Journal of Inorganic Chemistry

ChemPubSoc Europe

FULL PAPER

DOI:10.1002/ejic.201301271

Lanthanide Complexes with Tetradentate *N*,*N*′,*O*,*O*′-Dipyridyl-Based Ligands: Structure, Stability, and Photophysical Properties

Nataliya E. Borisova,*[a] Andrey A. Kostin,[a] Elizaveta A. Eroshkina,[a] Marina D. Reshetova,[a] Konstantin A. Lyssenko,[b] Evgenia N. Spodine,[c] and Lada N. Puntus[b,d]

Keywords: Lanthanides / N,O ligands / Structure elucidation / UV/Vis spectroscopy / Density functional calculations

A series of lanthanide(III) complexes (Ln = La to Lu) with 2,2′-bipyridyl-6,6′-dicarboxamide ligands were obtained. The X-ray structure of the di(*N*-ethylanilide) of 2,2′-bipyridyl-6,6′-dicarboxylic acid is reported. The structures of the amides in the gas phase were modeled by DFT calculations. The global minima of the structures on the potential energy surface (PES) strongly depend on the nature of the substituents on the amidic nitrogen atom. The UV/Vis titration results of three diamides of 2,2′-bipyridyl-6,6′-dicarboxylic acid with lanthanide(III) metal nitrates show the composition of the complexes formed and allow us to determine the binding constants. Compounds with a 1:1 metal-to-ligand ratio are formed with the three diamide ligands under study. The binding constants are high, $\log\beta_1$ being higher than 5.5. The values of the constants decrease from La^{III} to Lu^{III}. The first structures, obtained by single-crystal X-ray diffraction, for Gd^{III} and Tb^{III} complexes of 2,2′-bipyridyl-6,6′-dicarboxamide ligands are described. Decacoordinated metal ions are bonded by the tetradentate ligand and three bidentate nitrate groups. 2D ROESY experiments with La^{III}, Lu^{III}, and Eu^{III} complexes allow us to conclude that the structures of the complexes in solution are the same as those in the solid state. The photophysical properties of these Ln complexes were determined in the solid state at 77 and 300 K. Intense red and green luminescence was observed for both Eu and Tb complexes, and an intrinsic quantum yield of 90 % was determined for the europium complex.

Introduction

Atomic energy is a popular alternative for generating large-scale electric power without CO_2 emission.[1] Though the accidents at Chernobyl and Fukushima highlight problems with nuclear plant safety, the major long-term problem of nuclear energy is nuclear waste storage and accumulation. Current technologies are able to partially regenerate nuclear fuel but lead to the accumulation of long-living high-level nuclear waste (HLW).[2] Reducing nuclear waste levels requires the effective and selective separation of long-living fissile isotopes, particularly minor actinides (MAs), such as americium (Am) and curium (Cm), from the HLW for subsequent transmutation by neutron irradiation.[3] MAs possess physical and chemical properties similar to those of lanthanide (Ln) ions, which are also present in spent fuel. Thus, separating MAs from Ln^{III} is the key problem.

In recent years, the use of selective organic ligands to isolate target ions has become more promising. A number of potential organic molecules have been synthesized for this purpose, including dithiophosphinic acids,[4] diglycolic amides,[5] and polydentate nitrogen-containing extractants.[6] Although dithiophosphinic acids have very high separation factors (Am/Eu $> 10^4$), they are not oxidatively stable in aggressive nuclear wastes and, therefore, are not ideal. In contrast, polynitrogen aromatic ligands are more favorable since they can be chemically modified at many positions to alter the ligand behavior.[7] Studies of pure nitrogen-containing heterocyclic extractants show that increasing the number of nitrogen atoms enhances their affinity for americium.[6a] Triazinyl-containing nitrogen-rich compounds are also a good choice for selectively separating

[a] Chemistry Department, M. V. Lomonosov Moscow State University,
1 Leninskie Gory, 119991 Moscow, Russian Federation
E-mail: borisova.nataliya@gmail.com
http://fhmas.chem.msu.ru
[b] N. A. Nesmeyanov Institute of Organoelement Compounds, Vavilova st. 28, 119334 Moscow, Russia
[c] Faculty of Chemical and Pharmaceutical Sciences, University of Chile, Center for the Development of Nanoscience and Nanotechnology (CEDENNA),
Sergio Livingstone P. 1007, Independencia, Santiago, Chile
[d] Kotel'nikov Institute of Radio Engineering and Electronics of Russian Academy of Sciences,
Mokhovaya st. 11-7, 125009 Moscow, Russia

Supporting information for this article is available on the WWW under http://dx.doi.org/10.1002/ejic.201301271.

MAs and can function in solvents like octanol-1. However, extractants that can be used in fluorinated solvents (e.g., trifluoromethylphenyl sulfone or *m*-trifluoromethyl nitrobenzene) have not yet been developed.

We designed a heteropolydentate ligand that possesses two soft nitrogen-containing heterocycles and two carboxamide groups for binding actinides, which are slightly harder than lanthanides. We expected to achieve high selectivity for Am, and preliminary results showed that the synthesized ligands [diamides of 2,2′-bipyrydil-6,6′-dicarboxylic acid (DPDAs)] were highly selective for Am^{III} in comparison with Eu^{III}.[8] Moreover, ligand affinity to lanthanides decreased linearly with increasing atomic number of the lanthanide. The extracting ability of DPDAs heavily depends on the structure of their side amidic chain. The most effective extraction occurs when the amide contains both aromatic and aliphatic substituents as its amidic groups, and no extraction was observed when a long aliphatic diamide chain was used. We performed quantum chemical calculations on the structures of several DPDAs to determine how the side amidic group affected metal binding. In addition, we synthesized and analyzed the structure of the Ln–DPDA complexes that form in the organic phase. Stability constants for Ln ions (lanthanum to lutetium) were measured in the presence of several DPDA ligands to determine the effect of ionic radii on the stability of the DPDA complexes.

From another point of view, the luminescence of lanthanide ions is in the focus of intense research efforts because of the wide technical and analytical applications. The literature in this field is growing fast, and a number of reviews have been published during the last ten years to accumulate and analyze information in this popular area.[9] The most important applications of the photophysical properties of lanthanide ions are lighting (luminophores[10] and electroluminophores[11]) and bioanalytics (biochemical sensors[12] and medical imaging[9a,9c,13]). Moreover, photophysical properties are very important for the estimation of the further possible applications of new luminescent complexes. To shed light on the possible optical applications of lanthanide–DPDA complexes, we also investigated their photophysical properties in this work.

Results and Discussion

Structures of the 2,2′-Dipyridyl-6,6′-dicarboxamide Ligands

^{1}H NMR spectroscopic data show that all three DPDA molecules ($\mathbf{L_{Ph}}$, $\mathbf{L_{Bu2}}$, and $\mathbf{L_{Oct2}}$) possess highly symmetrical C_s geometry (Figures S1–S3). The two pyridine rings are equivalent, and the amide side arms have identical chemical shifts. These data indicate the existence of an inversion center in the ligands. Studying the restricted intramolecular rotations of the amide groups in [D_3]acetonitrile indicated moderate energy barriers (16.02 kcal/mol for $\mathbf{L_{Bu2}}$[8a] and 16.74 kcal/mol for $\mathbf{L_{Oct2}}$). For ligand $\mathbf{L_{Ph}}$, only one conformer with *cis*-orientation of the ethyl substituent was observed.[8a] This strongly supported the observation of the rotating-frame Overhauser effect (ROESY)[14] for ligand $\mathbf{L_{Ph}}$. The corresponding cross peak was found between the broad singlet of the amidic phenyl ring and the 3′-position of the pyridine ring (Figure S4).

The solid-state structure was determined for the $\mathbf{L_{Ph}}$ ligand (Figure 1, Tables S1 and S2). $\mathbf{L_{Ph}}$ possesses a center of symmetry at the C14–C14a bond of the bipyridyl moiety. The phenyl groups are *trans* in relation to the amide oxygen. The phenyl rings are located in close proximity to the pyridine rings of the bipyridyl unit, and the torsion angle C10–C9–N2–C1 is –14.5°. Due to steric hindrance, the dihedral angle of the bulky phenyl and pyridyl groups is 64°. The amide moieties significantly deviate from the bipyridyl plane; moreover, the carboxamide group is distorted from the planes of both the pyridine and the phenyl rings and has corresponding dihedral angles of 42° and 64°, respectively. Thus, there is no evidence for electronic conjugation between the two aromatic phenyl and pyridyl rings and the carboxamide group. Consequently, the energy of the rotational barrier of the carboxamide group is likely lower as a result of the CO–N bond. The crystal packing of $\mathbf{L_{Ph}}$ is described in Figure S5.

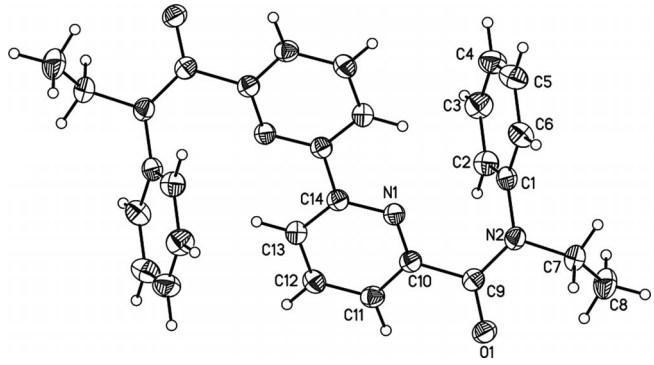

Figure 1. Molecular structure of $\mathbf{L_{Ph}}$, showing the atom numbering scheme. Displacement ellipsoids are drawn at the 50% probability level, and H atoms are shown as small spheres of arbitrary radius.

The calculated geometry of one potential energy surface (PES, see below) minimum for $\mathbf{L_{Ph}}$ was in good agreement with its solid-state structure. Therefore, $\mathbf{L_{Ph}}$ has a similar structure in both the solid state (X-ray crystallography data) and in solution (NMR spectroscopic data).

DFT Calculations for the Diamide Ligands

The structures of the amides were calculated by DFT. The following combinations of mutual orientations of coordinating *N*,*N*′,*O*,*O*′-groups are possible for the DPDA ligands: the *syn*,*syn*, *syn*,*anti*, and *anti*,*anti* orientations of the carbonyl groups of the amides with respect to the nitrogen atoms of the pyridine rings, and the *syn* and *anti* orientations of the nitrogen atoms of the pyridine rings with respect to each other (Scheme 1). The *s*-*s*-*s* conformation is the most preorganized for binding a metal ion, while the *a*-*a*-*a* conformer is the least preorganized. We calculated and compared energies and standard Gibbs free energies of formation for all possible isomers (Scheme 1).

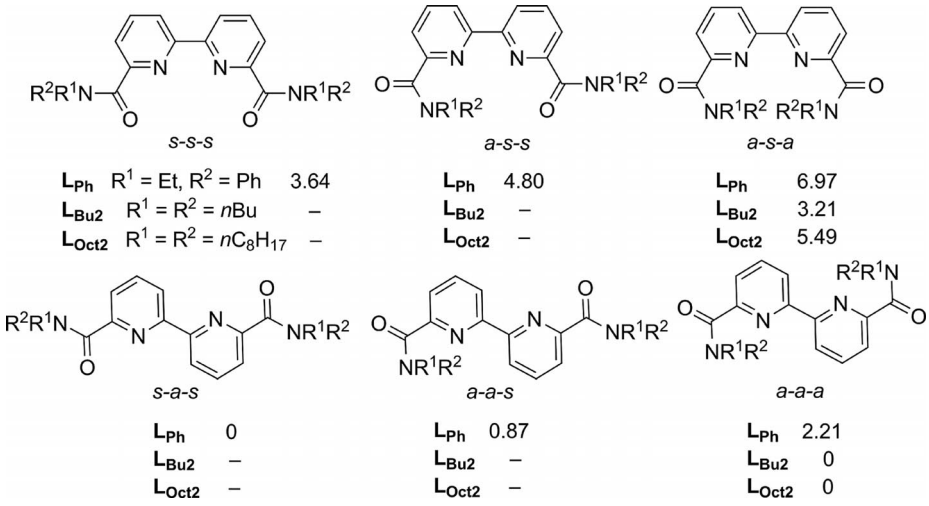

Scheme 1. Possible conformations of the DPDA ligands with their relative Gibbs free energies (in kcal/mol).

Minima on the PES for all six possible isomers were only observed for $\mathbf{L_{Ph}}$, which contains the phenyl substituent in the amide group. Two minima, corresponding to the *a-s-a* and *a-a-a* conformers, were observed for the tetraalkyl-substituted $\mathbf{L_{Oct2}}$ and $\mathbf{L_{Bu2}}$. The global PES minimum of $\mathbf{L_{Oct2}}$ and $\mathbf{L_{Bu2}}$ corresponds to the least preorganized conformer (*a-a-a*), and no minima correspond to the most preorganized conformation (*s-s-s*). The partially preorganized conformer (*s-a-s*) corresponds to the global PES minimum of $\mathbf{L_{Ph}}$. The *s-s-s* conformer is most prone to metal ion binding and its minimum energy is 3.64 kcal/mol higher than that of the *s-a-s* conformer. The *a-s-a* conformer has the highest PES minimum with 7 kcal/mol.

The geometry of the $\mathbf{L_{Ph}}$ *a-a-a* conformer was calculated for the gas phase and was found to be close to that of the molecule's X-ray structure (Table S2). For the tetraalkyl-substituted amides, the second PES minimum was calculated to be 3.21 and 5.49 kcal/mol higher than that of the main *a-a-a* conformer for $\mathbf{L_{Bu2}}$ and $\mathbf{L_{Oct2}}$, respectively. A geometrical analysis of the molecules corresponding to PES minima showed that, regardless of the amide substituents, pyridine rings are unfolded at 178–179° for *anti* conformers (Table S3). In contrast, the *syn* conformers have torsion angles of 30° between the two rings, which agrees more with the *gauche* conformation. Similarly, we obtained average angles of 135 ± 6° between the carbonyl groups and pyridine rings for *anti* conformers, regardless of the amide substituent. The average angle for the *syn* conformers, which was only found for $\mathbf{L_{Ph}}$, is 63 ± 6°, which also agrees with a *gauche* conformation.

As expected, the amide substituents substantially affect the ligand geometry. For all tetraalkyl-substituted amides ($\mathbf{L_{Bu2}}$ and $\mathbf{L_{Oct2}}$), the carboxamide groups and α-carbon atoms of the substituents lie in one plane in all conformations, and the corresponding torsion angles never exceed 2°. For the anilide ($\mathbf{L_{Ph}}$), the aromatic rings form a 60° angle with the carboxamide plane, and the orientation depends on those of the carbonyl group and pyridine ring. All *syn* conformations of the carbonyl group have *trans*-phenyl substituents with respect to the pseudo double amide C–N bond. In contrast, the *anti* conformations of the carbonyl group have *cis*-phenyl groups. This was clearly reflected in the torsion angles between the C=O bond of the carbonyl group and the N–C bond of the phenyl substituent (Table S3). The *syn* and *anti* torsion angles are 168 ± 4° and 3 ± 4°, respectively; the torsion angle reaches 26.33° in only one case (*a-s-a*). Neither the amide substituent nor the conformational behavior affects the heteroatom charges (Table S3).

The amide with an aromatic substituent ($\mathbf{L_{Ph}}$) is more preorganized for binding metal ions than its tetraalkyl-substituted analogs ($\mathbf{L_{Oct2}}$ and $\mathbf{L_{Bu2}}$). The energy differences between the conformers are not high and do not exceed 5.5 kcal/mol for $\mathbf{L_{Oct2}}$ and $\mathbf{L_{Bu2}}$ and 7.5 kcal/mol for $\mathbf{L_{Ph}}$. However, such low energy values cannot explain the considerable difference in extraction ability we observed. Thus, we also studied the rotational barriers of the pyridine rings and amide groups. The rotation of the pyridine rings about the C–C bond is similar for all three amides (Figure S6). The maximum rotational barriers of the pyridine rings are 9.25, 6.15, and 6.67 kcal/mol for $\mathbf{L_{Ph}}$, $\mathbf{L_{Bu2}}$, and $\mathbf{L_{Oct2}}$, respectively. In contrast, the rotation of the carboxamide group about the C–C bond is heavily dependent on the amide side chain and is characterized by significant rotational barriers (Figure S7). The barrier is much higher for the tetraalkyl-substituted amides (21.05 kcal/mol for $\mathbf{L_{Oct2}}$ and 17.34 kcal/mol for $\mathbf{L_{Bu2}}$) than that for the anilide amide (14.11 kcal/mol for $\mathbf{L_{Ph}}$). This distribution of rotational barrier energy is similar to the changes in extraction ability for this series of amides. $\mathbf{L_{Ph}}$ has much higher distribution coefficients compared to $\mathbf{L_{Bu2}}$, while $\mathbf{L_{Oct2}}$ does not extract Am or Eu. The *a-a-a* conformer, which is the least preorganized for metal ion binding, corresponds to the global minimum for tetraalkyl-substituted amides and has to overcome

a considerable energy barrier (the rotation of the carboxamide group) to bind metal ions. The anilide $\mathbf{L_{Ph}}$ has a global minimum corresponding to the partially preorganized *s-a-s* conformer, and only a slight energy barrier (the unfolding of the pyridine rings) needs to be overcome for metal ion binding.

This reasoning is supported by knowing the energy required for binding-site reorganization for each ligand. Higher ligand affinity is closely related with ligand conformity and complementarity.[15] The latter is considered as the energy required for structural reorganization of the ligand during the complexation. We calculated the total energy of binding-site reorganization by using the difference between the global PES minimum and the energy of the bound ligand (see Experimental Section). All the ligands had nonzero energies for binding-site reorganization for binding a Eu ion. The lowest reorganization energy required was observed for $\mathbf{L_{Ph}}$ (17.40 kcal/mol), and more reorganization energy was required for $\mathbf{L_{Bu2}}$ and $\mathbf{L_{Oct2}}$ (21.48 and 23.45 kcal/mol, respectively). Thus, $\mathbf{L_{Ph}}$ is more preorganized for binding Eu^{III} and has lower energy barriers to overcome, resulting in a better extraction ability compared to $\mathbf{L_{Bu2}}$ and $\mathbf{L_{Oct2}}$. Moreover, this further explains why $\mathbf{L_{Oct2}}$, which is the least preorganized, cannot extract metal ions.

Ln^{III} Complexes with L_{Ph}

We studied complexes of $\mathbf{L_{Ph}}$, the most promising extractant, with Ln^{III} to understand the differences between Am^{III} and Eu^{III} extraction by the DPDA ligands. These complexes are directly synthesized by reacting hydrated nitrates of Ln^{III} with $\mathbf{L_{Ph}}$ in acetonitrile heated to reflux and have the same $Ln\mathbf{L_{Ph}}(NO_3)_3$ composition for all lanthanide ions (La^{III} to Lu^{III}; Scheme 2).

Complex yields decreased from lanthanum (70%) to samarium and europium (61–65%) and returned to 70% from gadolinium to ytterbium and lutetium. The complexes were characterized by standard spectroscopic techniques; the infrared spectra of the synthesized complexes were almost identical, and the spectra for all complexes significantly differed from those of the free ligand. The band near 1610 cm^{-1} corresponding to the first amide band is very sensitive for metal binding. The spectra of the observed amide bands decreased from 1639 cm^{-1} for the free ligand to 1610 cm^{-1} for the corresponding complexes, which confirms the complexation of metal ions with the amidic oxygen atom. N=O bands for NO_3 anions were observed near 1456 cm^{-1} for all of complexes. Less intense bands, which correspond to symmetrical and asymmetrical deformation of the O–N–O vibrations in the NO_3 anions, were also observed. Mass spectra obtained by MALDI-TOF showed only one ion ($Ln\mathbf{L_{Ph}}[NO_3]_2^+$) in the laser desorption-ionization mode. Secondary peaks originating from the exchange reaction between nitrate and cinnamic acid anions were observed in the MALDI mode in the presence of a cinnamic acid matrix. All mass spectra showed peaks derived from mononuclear complexes of $Ln\mathbf{L_{Ph}}(NO_3)_3$.

X-ray structures of the complexes show monometallic complexes in which the metal coordinates with the tetradentate DPDA ligand and the three bidentate nitrate ions. Figure 2 shows the structure of the complex with Gd^{III}, which is isostructural with the complexes with Pr^{III}, Nd^{III}, and Tb^{III}, together with the atom numbering scheme. Selected bond lengths and angles are given in Table 1 (the crystal data and structural refinements are presented in Table S1, interatomic distances and angles are in Table S4).

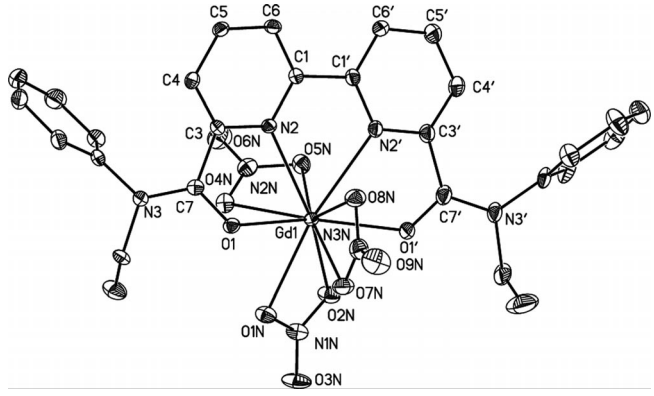

Figure 2. Molecular structure of complex $Gd\mathbf{L_{Ph}}(NO_3)_3$, showing the atom numbering scheme.

Table 1. Comparison of the interatomic distances (Å) and angles (°) in the coordination sphere of the metal ions for complexes with the $\mathbf{L_{Ph}}$ ligand.

Bonds/angles	$Pr\mathbf{L_{Ph}}(NO_3)_3$	$Nd\mathbf{L_{Ph}}(NO_3)_3$	$Gd\mathbf{L_{Ph}}(NO_3)_3$	$Tb\mathbf{L_{Ph}}(NO_3)_3$
M–O1	2.490(2)	2.481(1)	2.414(2)	2.402(3)
M–O1′	2.414(2)	2.409(1)	2.346(2)	2.325(3)
$d_{M-O1} - d_{M-O1'}$	0.075(2)	0.072(1)	0.068(2)	0.077(3)
M–N1	2.623(2)	2.605(2)	2.530(2)	2.514(3)
M–N1′	2.694(2)	2.683(2)	2.625(2)	2.611(3)
$d_{M-N1} - d_{M-N1'}$	0.071(2)	0.078(2)	0.095(2)	0.097(3)
O1–M–O1′	162.09(6)	161.48(5)	153.11(6)	154.66(8)
N1–M–N1′	61.08(6)	61.30(5)	52.36(6)	62.65(6)

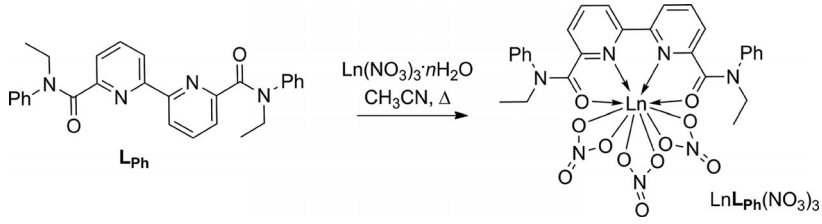

Scheme 2. Synthesis of $Ln\mathbf{L_{Ph}}(NO_3)_3$.

Table 2. Chemical shifts (ppm) of the protons of the $\mathbf{L_{Ph}}$ ligand and the corresponding Ln^{III} complexes.

	CH_3	CH_2	$CH_{5'-Py}$	CH_{Ph}	$CH_{4'-Py}$	$CH_{3'-Py}$
$\mathbf{L_{Ph}}$	t 1.18	q 3.93	m 7.03–7.32		t 7.74	d 7.57
$La\mathbf{L_{Ph}}(NO_3)_3$	t 1.26	q 4.09	d 6.99	m 7.31–7.53	t 7.80	d 8.19
$Eu\mathbf{L_{Ph}}(NO_3)_3$	b room temp. –0.27	br.s. 2.34	br.d. 3.42	br.s. 7.39	b room temp. 5.29	br.d. 3.64
$Lu\mathbf{L_{Ph}}(NO_3)_3$	t 1.29	q 4.10	d 6.85	m 7.38–7.45 7.48–7.58	t 7.90	d 8.30

The coordination sphere of the metal ion can be described as a distorted two-capped square antiprism in which N2, O8N, O1′, O5N and O1, O4N, O2N, O7N define two distorted square faces of the antiprism; the faces are capped with N2′ and O1N, respectively. The two tetragonal faces are nearly parallel (1.2–1.7°) and are separated by approximately 2.1 Å. The Ln atom is located at the middle of the distance between the faces. The N2, O8N, O1′, O5N face is capped with the N2′ pyridine atom, which is placed under the center of the face.

The second face is capped with the oxygen atom O1N from the nitrate ion – notable is that the second oxygen atom, O2N, of this nitrate ion lies in the square face, and this shifts the O2N cap from the center to the square as a result of the short interatomic distance in the nitrate. The angle between the Ln–O2N bond and the perpendicular distance to the face plane is about 15°. Such coordination of the metal atom leads to the inequivalence of the two pyridine nitrogen atoms of the bipyridine unit and the two oxygen atoms of the carboxamide groups because of steric hindrance. This steric hindrance between NO_3 and carboxamide groups causes the significant difference in torsion angles: O1–C7–C3–N2 25.4–28.9° and O1′–C7′–C3′–N2′ 7.5–7.2. As a consequence, the M–O1′ bond in all members of this isostructural series is systematically shorter than M–O1 while the M–N2′ bond is longer than M–N2. The difference in M–N and M–O bonds for these formally equivalent parts of the ligand is almost independent from the nature of the metal atom and therefore also from the lanthanide contraction. The independence of the above differences from the nature of the metal center is probably a result of variations in the torsion angle N2–C1–C1′–N2′, which are equal to 5.0 and 4.6° for Nd and Pr complexes and increase up to 12.8 and 11.0° for Gd and Tb. Thus, the strength of the metal-to-ligand bonding is mostly governed by the steric repulsion between the carboxamide groups, and the nitrate ligand and is less affected by lanthanide radii.

NMR spectra were recorded for the diamagnetic La^{III} and Lu^{III} and for the Eu^{III} complexes (Table 2, Figures S8 and S9). The diamagnetic spectra have similar peak patterns and differ in only chemical shifts. The 3′- and 4′-pyridine proton peaks of the ligand are shielded as a result of metal ion binding. The deshielded cone of the neighboring phenyl ring causes an unexpected shift up for the 5′-pyridine ring protons. Complexes with metals of a higher atomic number shield more the pyridine protons.

The ROESY[14] spectrum was recorded for the diamagnetic complexes: cross peaks occur between the 5′-pyridine ring proton and the *o*-protons of the phenyl ring (Figures S10–S12). This confirms the conclusion that these protons are deshielded in the complexes compared to those in the free ligand. Together, these data show that the complexes maintain the same conformation in solution as they have in crystal form.

Formation Constants of $LnDPDA(NO_3)_3$ Complexes in Solution

NMR spectroscopic data and the chemical syntheses provided the initial evidence of complex stability in acetonitrile solution. UV/Vis spectrophotometric titration was used to quantitatively assess the ability of the ligand to bind Ln ions in acetonitrile solution (see Supporting Information). The absorbance spectrum of the ligands in acetonitrile is characterized by two broad bands in the UV range (near 293 and 245 nm). A new band near 310 nm with good isosbestic behavior was observed as increasing amounts of metal salt were added. On the basis of our X-ray and NMR spectroscopic data, we expected complexes to form at a 1:1 stoichiometric ratio in solution. The 1:1 ratio was observed for all the metals, and the titration curves increased smoothly with a marked endpoint at a M/L value of 1:1.

The binding constants β were calculated according to Equations (1), (2), (3), and (4):

$$[ML] = \frac{Abs - \varepsilon_L \cdot c_L}{\varepsilon_{ML} - \varepsilon_L} \quad (1)$$

$$[M] = C_M - [ML] \quad (2)$$

$$[L] = C_L - [ML] \quad (3)$$

$$\beta = \frac{[LM(NO_3)_3]}{[L][M(NO_3)_3]} \quad (4)$$

where *Abs* is absorbance at the chosen wavelength, ε_{ML} is the molar absorbance coefficient of the $ML(NO_3)_3$ complex at the chosen wavelength, and c_L and c_M are total ligand and metal salt concentrations, respectively. $\log\beta$ values for the Ln^{III} complexes are shown in Table 3 and Figure S13. All the DPDA ligands have high affinities for Ln^{III} ions with $\log\beta$ values greater than 5.5. These values are lower than the $\log\beta_1$ values measured for the related 2,6-pyridinedicarboxylic acid (PDAs: $\mathbf{Py_{iPr2}}$ and $\mathbf{Py_{Et2}}$) diamides (Table 3). The $\mathbf{L_{Ph}}$ and $\mathbf{L_{Oct2}}$ constants do not vary as much between lanthanide ions, and $\mathbf{L_{Oct2}}$ has the highest constants. The binding constants of both $\mathbf{L_{Ph}}$ and $\mathbf{L_{Oct2}}$ tend to decrease from lanthanum to lutetium, but the decrease is not constant. $\mathbf{L_{Bu2}}$ has similar binding constants for all lanthanide ions. Generally, the binding constant is lower

for cerium(III) than lanthanum(III) and praseodymium(III) (Table 3) for all three ligands, and the binding constants for the tetraalkyl-substituted ligands have the smallest value for cerium(III). If the anomalous behavior of cerium is excluded, we can conclude that the DPDA ligands bind metal ions with larger ionic radii better.

Table 3. Logβ_1 values (with accuracies in parentheses) for the binding of the PDA and DPDA ligands with lanthanide(III) ions in acetonitrile.

M	$\mathbf{L_{Ph}}$	$\mathbf{L_{Bu2}}$	$\mathbf{L_{Oct2}}$	$\mathbf{Py_{iPr2}}$[16]	$\mathbf{Py_{Et2}}$[17]	$\mathbf{Py_{Bn2}}$[16]
La	6.2(2)	5.5(3)	6.7(2)	7.8(5)	7.4(3)	5.4(5)
Ce	5.6(1)	5.3(1)	5.9(2)	7.4(4)	7.6(3)	
Pr	5.9(1)	5.1(3)	6.5(4)	8.0(6)	7.6(3)	
Nd	5.9(1)	5.7(2)	6.6(2)	7.7(5)	7.5(3)	
Sm	5.7(1)	5.3(3)	6.2(1)	8.5(6)	7.3(3)	
Eu	5.6(1)	6.1(3)	6.2(1)	8.3(6)	8.3(3)	4.9(5)
Gd	5.7(1)	5.2(3)	6.2(1)	7.9(7)	7.9(3)	
Tb	5.7(1)	5.5(2)	6.1(1)	7.6(6)	8.2(3)	
Dy	5.7(1)	5.1(2)	6.3(1)	7.7(5)	7.5(3)	
Ho	5.7(2)	5.4(3)	6.3(1)	8.3(6)	7.3(4)	
Er	5.4(1)	6.3(2)	6.3(2)	8.3(5)	7.7(4)	
Tm	5.9(2)	5.4(3)	6.5(1)	7.9(6)	8.5(3)	
Yb	5.6(2)	5.9(3)	6.4(1)	7.7(4)	8.5(3)	
Lu	5.5(2)	5.7(4)	6.4(1)	7.6(4)	8.1(3)	5.3(5)

In contrast to the DPDA ligands, PDA ligands (Scheme 3) complex with hydrated triflates of Ln^{III} at 1:1, 1:2, and 1:3 ratios in acetonitrile (Table 3).[16,17] In general, β_1 values of the PDA ligands are higher than those of the bipyridyl analogs, except for that of $\mathbf{Py_{Bn2}}$, which is very close to that of $\mathbf{L_{Oct2}}$. Logβ1 values of $\mathbf{Py_{Et2}}$ and $\mathbf{Py_{iPr2}}$ are comparable and experience an electrostatic trend (i.e., a slight increase in binding constants with decreasing metal ion size), as expected, which results from the contraction of ionic radii along the lanthanide series.[16]

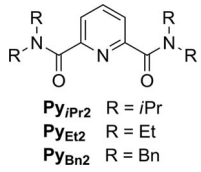

$\mathbf{Py_{iPr2}}$ R = *i*Pr
$\mathbf{Py_{Et2}}$ R = Et
$\mathbf{Py_{Bn2}}$ R = Bn

Scheme 3. Structure of the PDA ligands, whose complexation with Ln^{III} was studied.

Photophysical Properties of $LnDPDA(NO_3)_3$ Complexes in the Solid State

Upon excitation at the absorption band (330 nm) of ligand $\mathbf{L_{ph}}$, the emission spectra of complex $Eu\mathbf{L_{ph}}(NO_3)_3$ (at 77 and 300 K) show the typical narrow bands corresponding to the Eu^{III} $^5D_0\rightarrow{}^7F_J$ (J = 0–4) transitions (Figure 3). A forbidden $^5D_0\rightarrow{}^7F_0$ transition of the Eu^{III} situated at 580.6 nm and presented by a symmetric line is nondegenerated in this complex and indicates the presence of one type of Eu environment in the crystal. The magnetic dipole $^5D_0\rightarrow{}^7F_1$ transition centered at 593 nm is largely independent of the chemical environment of europium. An electric dipole $^5D_0\rightarrow{}^7F_2$ transition with the most intense Stark component at 616.5 nm is extremely sensitive to the symmetry of the coordination sphere and is therefore called *hypersensitive*. The ratio of the integrated intensity of the $^5D_0\rightarrow{}^7F_2$ transition to that of the $^5D_0\rightarrow{}^7F_1$ transition is a measure for the symmetry of the coordination sphere.[18] In a centrosymmetric environment, the magnetic dipole $^5D_0\rightarrow{}^7F_1$ transition dominates and the ratio is less than 1, while the distortion of the symmetry around the ion causes an enhancement in the intensity of the $^5D_0\rightarrow{}^7F_2$ transition. In complex $Eu\mathbf{L_{ph}}(NO_3)_3$ this ratio is approximately 7, which indicates a significant deviation from the inversion center. General splittings for the ^7F_J states, where J = 1, 2, 4, are about 190, 200, and 500 cm^{-1}, respectively. Interestingly, the general splitting of the $^7F_4$ manifold (range 680–705 nm) is similar to that for $Eu(NO_3)_3Phen_2$ (530 cm^{-1}) and correlates well with CN = 10 and the pronounced contribution of the nitrate groups to the ligand field (charge distribution around Eu^{III}).[19] The luminescence decay curves obtained from the time-resolved luminescence experiments could be fitted monoexponentially with the time constants in the range of microseconds. The luminescence lifetimes of the $^5D_0$ level in $Eu\mathbf{L_{ph}}(NO_3)_3$ at 77 and 300 K are 1.77 ± 0.03 and 1.70 ± 0.02 ms, respectively. These values are in line with the absence of solvent molecules in the europium coordination sphere in accordance with X-ray diffraction data.

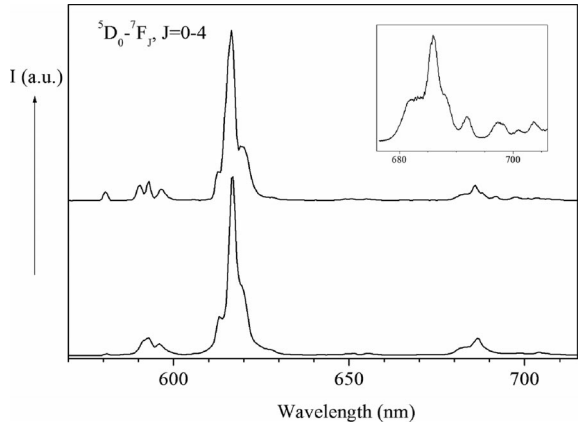

Figure 3. Luminescence spectra of complex $Eu\mathbf{L_{ph}}(NO_3)_3$ at (a) 77 and (b) 300 K. The region of the $^5D_0\rightarrow{}^7F_4$ transition is presented in the inset.

In the luminescence spectrum of the Tb^{III}-containing complex $Tb\mathbf{L_{ph}}(NO_3)_3$, the following transitions could be detected (Figure 4): $^5D_4\rightarrow{}^7F_6$ (480–500 nm), $^5D_4\rightarrow{}^7F_5$ (535–555 nm), $^5D_4\rightarrow{}^7F_4$ (575–595 nm), $^5D_4\rightarrow{}^7F_3$ (610–630 nm), $^5D_4\rightarrow{}^7F_2$ (640–660 nm), $^5D_4\rightarrow{}^7F_1$ (660–675 nm), $^5D_4\rightarrow{}^7F_0$ (675–685 nm). The last three transitions have low intensity as expected. The $^5D_4\rightarrow{}^7F_5$ transition is the most prominent and accounts for approximately 60% of the total emitted intensity. The luminescence lifetimes of the $^5D_4$ level in $Tb\mathbf{L_{ph}}(NO_3)_3$ at 77 and 300 K are 1.85 ± 0.03 and 0.41 ± 0.02 ms, respectively. Such difference in the observed values of the lifetimes may be caused by the presence of an energy back transfer process (see below).

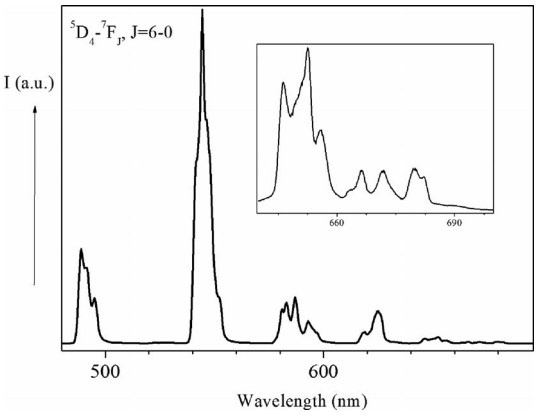

Figure 4. Luminescence spectrum of Tb$\mathbf{L_{ph}}(NO_3)_3$ at 77 K, the region of the $^5D_4 \rightarrow {}^7F_J$ (J = 0–2) transitions is presented in the inset.

Luminescence sensitization in lanthanide-containing systems by energy transfer from ligand excited states to the resonance states of Ln^{III} can occur in different ways. The favorite mechanism, in a simplified version, involves ligand excitation by the absorption of ultraviolet energy to an excited singlet state, followed by energy migration, via nonradiative intersystem crossing, to a ligand triplet state [$\Delta E_1 = E(S_1) - E(T)$], and energy transfer from the triplet state to a resonance state of the Ln^{III} ion, from which the emission occurs [$\Delta E_2 = E(T) - E(^5D_J)$, where J = 0 and J = 6 for the europium and terbium ions, respectively].[20] In principle, direct transfer from the singlet S_1 state is also possible but seems to be less important for Eu than for Tb.[21] Moreover, in the case of europium complexes, a photon-induced electron transfer (ligand-to-metal charge transfer, LMCT) may also play a role in the deactivation of the singlet excited state. Indeed, instead of radiative decay to the ground state, or intersystem crossing to the triplet state, an electron is transferred to the Eu^{III} ion upon excitation of the antenna into its singlet excited state, resulting in the transient formation of an antenna radical cation and Eu^{II}.[22] One of the reasons for the possible occurrence of this competing process is the low reduction potential of Eu^{III} in comparison with other trivalent lanthanide ions.[23]

Since the Gd^{III} ion has no energy levels below 310 nm/32000 cm^{-1}, it can be used for the estimation of the energy of the excited states of the coordinated ligands. The energies of the lowest excited singlet (S_1) and triplet (T) states of the $\mathbf{L_{ph}}$ ligand, 340 nm/29410 cm^{-1} and 470 nm/21300 cm^{-1}, respectively, were determined from the luminescence and phosphorescence spectra of Gd$\mathbf{L_{ph}}(NO_3)_3$. Additionally, the presence of emission from the $^5D_1$ state in the luminescence spectrum of complex Eu$\mathbf{L_{ph}}(NO_3)_3$, which converts nonradiatively into the $^5D_0$ state and radiatively to the ^7F_J manifold, is logical for the sensitized Eu^{III} emission in the case when the donating triplet level of $\mathbf{L_{ph}}$ is above the $^5D_1$ level of Eu^{III}.

Scanning the excitation wavelength while monitoring the intensity of the Eu^{III} or Tb^{III} emission (613 or 545 nm, the strongest component of the $^5D_0 \rightarrow {}^7F_2$ or $^5D_4 \rightarrow {}^7F_5$ transition, respectively) shows which transitions from the ground state directly or indirectly lead to the population of the first excited state of the lanthanide ion. The excitation spectra of complexes Tb$\mathbf{L_{ph}}(NO_3)_3$ and Eu$\mathbf{L_{ph}}(NO_3)_3$ (Figure 5) display, in addition to narrow f–f transitions, a broad band extending from 250 to 350 nm with two intense components at 270 nm (37040 cm^{-1}) and 340 nm (29410 cm^{-1}). The first component is attributed to the π–π* transition of the $\mathbf{L_{ph}}$ ligand, while the second one is the first excited singlet state (S_1) of this ligand. An additional broad band centered at 380 nm/26315 cm^{-1} with a low-frequency edge at approximately 450 nm/22200 cm^{-1} is observed in the excitation spectra of the Eu complex. Since a weak broad band extending to approximately 410 nm is observed in a similar region of the excitation spectra of the Tb complex, this band cannot be assigned to an LMCT state but to an intraligand charge-transfer (ILCT) state. The origin of the ILCT state can be tentatively explained to some extent by the asymmetry of the $\mathbf{L_{ph}}$ ligand, in which one part has a stronger bond with the Ln^{III} ion owing to the C=O bond while the other part of the ligand has a stronger Eu–N bond. Similar excitation spectra containing ILCT bands were observed for lanthanide complexes with pyridylcarboxylic and dicarboxylic acids.[24] The difference observed in the position of a long-wavelength edge of the above weak broad band between the excitation spectra of the Eu and Tb complexes (410 and 450 nm, respectively) indicates the presence other additional band in the Eu case. Since this band is absent in the same part of the excitation spectra of the terbium complex it can be assigned to the Ligand→Eu^{3+} charge-transfer state (LMCT state). Because the nitrate groups have high electronegativity and typically do not form the additional excited state in the excitation spectra,[25] this charge-transfer state is mostly formed by the $\mathbf{L_{ph}}$ ligand. Taking into account 420 nm/23810 cm^{-1} as the energy of this charge-transfer state, the electronegativity of Eu^{III}, uncorrected for spin correlation, $\chi_{uncorr}(Eu)$, is

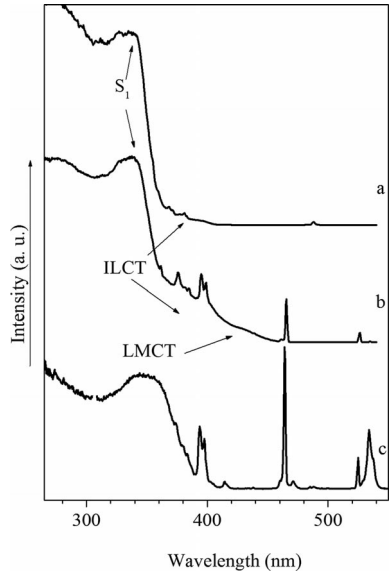

Figure 5. Excitation spectra of complexes Tb$\mathbf{L_{ph}}(NO_3)_3$ at 77 K (a) and Eu$\mathbf{L_{ph}}(NO_3)_3$ at 77 (b) and 300 K (c).

1.99,[26] and the energy of the charge-transfer state, E_{CTS}, is approximately 30000[$\chi_{opt}(X) - \chi_{uncorr}(Eu)$] cm^{-1}.[27] The optical electronegativity of the $\mathbf{L_{ph}}$ ligand, χ_{opt}, is 1.2. Therefore, the LMCT state observed is formed mostly by the $\mathbf{L_{ph}}\rightarrow Eu^{3+}$ charge transfer.

The information gained from the above analysis of the energy-transfer process may be summarized as follows: The energy difference between the S_1 and T states, denoted as the first energy gap (ΔE_1), amounts to 8135 cm^{-1}, which remarkably exceeds the optimum value for effective intersystem conversion (ca. 5000 cm^{-1}[28]). The second energy gap (ΔE_2, energy difference between the T and $^5D_0$ or $^5D_4$ levels for the Eu and Tb complexes, respectively) amounts to approximately 4000 and 800 cm^{-1}, respectively. Such a small value of the ΔE_2 along with the shortening lifetime of the $^5D_4$ level at 300 K (0.41 ± 0.02 ms) indicates an energy back transfer process, which promotes luminescence quenching in complex $Tb\mathbf{L_{ph}}(NO_3)_3$. The intrinsic quantum yield of the europium-centered emission calculated by means of Werts' formula[29] for complex $Eu\mathbf{L_{ph}}(NO_3)_3$ is Q_{Eu}^{Eu} = 90%, which is reasonable when we take into account the contents of the europium coordination sphere. Therefore, the energy migration process in the studied Eu system can be illustrated by the simplified diagram given in Figure 6.

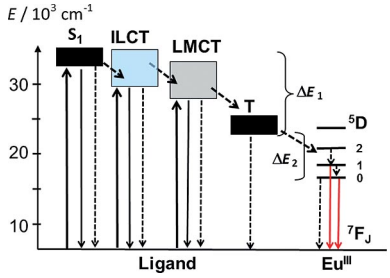

Figure 6. Simplified diagram of the energy migration processes in the considered complexes (S_1 = singlet state; T = triplet state; ILCT = intraligand charge-transfer state; LMCT = ligand-to-metal charge-transfer state; dotted and solid lines represent nonradiative and radiative processes, respectively).

Conclusions

The DPDA ligands studied here have a variety of extraction efficiencies and selectivities.[8] The most effective extractant is $\mathbf{L_{Ph}}$. The protons of its two pyridine rings have the same chemical shifts, indicating highly symmetrical bipyridyl C_s geometry in solution, while the amidic phenyl ring was shown to be located near the pyridine ring. These geometries were confirmed by DFT calculations for gas-phase conformations; the global PES minimum corresponded with the *s-a-s* conformer, while the next lowest PES corresponded with the *a-s-s* conformer. In contrast, the amidic groups are unfolded in the solid state with the oxygen atom located near the pyridine ring; thus, the molecule is not as preorganized for metal ion binding in this state. The solution and gas-phase structures of the other DPDA ligands ($\mathbf{L_{Bu2}}$ and $\mathbf{L_{Oct2}}$) were similar to that of $\mathbf{L_{Ph}}$, except that fewer PES minima were found. The global minima for these other ligands corresponded to the *a-a-a* conformer. $\mathbf{L_{Ph}}$ is more preorganized than the other DPDAs; this, with the knowledge that it has lower rotational barriers to overcome, makes $\mathbf{L_{Ph}}$ the better choice for metal ion binding.

The $\mathbf{L_{Ph}}$ ligand easily forms complexes with Ln^{III} ions. The metals coordinate with the tetradentate DPDA ligand and three nitrate ions, and the complexes of Gd^{III} and Tb^{III} have the same structures in solution as those in the solid state. The binding constants of the DPDA ligands with Ln^{III} are high with $\log\beta_1$ values greater than 5.5. The binding constants slightly decrease from lanthanum to lutetium and are less affected by the difference in amide substituents between the ligands.

The photophysical properties of the Ln complexes synthesized correlate well with their structure and with the peculiarities of the chemical bonding pattern in the inner coordination sphere. In particular, the origin of the ILCT state could be explained to some extent by the asymmetry of the $\mathbf{L_{ph}}$ ligand, in which one part has a stronger bond with the Ln^{III} ion owing to the C=O bond while the other part of the ligand has a stronger Eu–N bond. Moreover, the relatively low value of optical electronegativity obtained for the $\mathbf{L_{ph}}$ ligand should be taken into account while designing new lanthanide-containing optical systems, as this can lead to the appearance of a low-lying LMCT state. A detailed analysis of the energy-migration process shows that the $\mathbf{L_{ph}}$ ligand plays a shielding role to protect the Ln coordination sphere from any solvent molecules and has a broad channel for excitation, which can be useful in obtaining highly luminescent complexes with other Ln ions.

Experimental Section

General: The NMR spectra were measured with a BRUKER AVANCE-600 MHz NMR spectrometer at 24 °C. For dynamic NMR experiments, ^1H NMR spectra were recorded at 400.13 MHz with a BRUKER "Avance400" instrument in approximately 0.2 mol/L solutions in [D_8]toluene and CD_3CN, in 5 mm probe tubes at different temperatures (with the solvent as internal reference). IR spectra were recorded with a Nicolet FTIR spectrometer with samples in Nujol or KBr pellets. Mass spectra were obtained with a MALDI-TOF Reflex 3 instrument (BRUKER) in the positive ion mode (UV laser, 337 nm) with use of cinnamic acid as matrix. All of the reagents and solvents were obtained from commercial sources.

X-ray Structure Determination: Data collection was performed with Bruker Smart Apex (for $\mathbf{L_{Ph}}$) and SMART APEX II CCD (for Ln^{III} complexes) diffractometers. Reflection indexing, Lorentz-polarization correction, peak integration, and background determination were carried out with the Bruker SAINTPLUS[30] program. Empirical multiscan absorption corrections were performed by using equivalent reflections with the program SADABS.[31] The structure was solved and refined against F^2 by full-matrix least-squares techniques with the SHELXTL software package.[32] Crystallographic data and details of data collection are listed in Tables S1–S3 in the Supporting Information, and the diamide crys-

tal packing is shown in Figure S1. CCDC-930542 [for $\mathbf{L_{Ph}}$], -977838 [for $Tb\mathbf{L_{Ph}}(NO_3)_3$], -961723 [for $Gd\mathbf{L_{Ph}}(NO_3)_3$], -977836 [for $Nd\mathbf{L_{Ph}}(NO_3)_3$], and -977837 [for $Pr\mathbf{L_{Ph}}(NO_3)_3$] contain the supplementary crystallographic data for this paper. These data can be obtained free of charge from The Cambridge Crystallographic Data Centre via www.ccdc.cam.ac.uk/data_request/cif.

Computation Details: All calculations were carried out with the PRIRODA quantum chemistry program.[33] The gradient-corrected exchange-correlation Perdew, Burke, and Ernzerhof (PBE) functional[34] was used for the calculations. The efficient resolution of identity (RI) and parallel implementation of evaluating both Coulomb and exchange-correlation integrals with optimized fitting Gaussian basis sets in the PRIRODA code permits the performance of calculations of the molecular systems with a large number of basis functions.[33] A large integration grid (which comprises about 800000 points over calculated molecules) with a 5×10^{-9} accuracy parameter of the adaptively generated grid was used. This parameter is responsible for the precision of the exchange-correlation energy per atom. The 10^{-7} threshold on the orbital gradients at the energy calculations tag and the 10^{-5} threshold on the molecular gradient at the geometry optimization procedure were employed. In all calculations, the spin-restricted formalism was chosen. For all atoms except hydrogen, Stevens–Basch–Krauss (SBK) effective core pseudopotentials were used.[35] The valence shells were described by basis sets with the following contraction schemes [311/1] on H; [311/311/11] on C, N, and O. This basis set is denoted as SBK-TZ. The energy of the ligand bound by the Eu^{III} ion was calculated as proposed in ref.[15b] For the calculation of Eu complexes, we used the scalar-relativistic theory[36] and the relativistic full-electron basis sets L1[37] ([2,1]/[6,2] for H; [3,2,1]/[10,7,3] for C, N, and O; [9,8,6,3,1]/[30,29,20,14,6] for Eu). All geometries for the reacting species and transition states were completely optimized without any symmetry constraints. Systematic vibrational analysis was performed to confirm whether an optimized geometry corresponds to a transition state with only one imaginary frequency or to a local minimum without an imaginary frequency. Zero-point-vibrational-energy (ZPVE) corrections were taken into account in calculating the energetics of the reaction pathways. The rigid rotor and harmonic oscillator models were used for evaluation of the temperature (at 298 K) and entropy corrections for subsequent calculation of the Gibbs free energies of the processes under discussion. The same method and program have been successfully used earlier for the study of the mechanism of the catalytic oxidation of benzyl alcohol by the copper complex of the polymer 2,2′-bipyridyl-containing ligand.[38]

Photophysical Study: Luminescence measurements (spectra and lifetimes) were recorded with a Fluorolog FL 3–22 spectrometer from Horiba–Jobin–Yvon–Spex at 293 and 77 K. Phosphorescence lifetimes (τ) were measured with samples put into quartz capillaries; they are averages of at least three independent measurements. The decays were monitored at the maxima of the emission spectra. The single or bi-exponential decays were analyzed with Origin® 7.0.

General Method for the Preparation of the L_{Ph} Complexes of Lanthanides: A mixture of lanthanide trinitrate hydrate (0.52 mmol) with L_{Ph} (0.52 mmol) in dry acetonitrile (80 mL) was heated to reflux until complete dissolution of the starting ligand occurred. After cooling of the reaction mixture, large crystals of the complex were collected and dried. The mother liquor was collected and reduced in volume twice under vacuum, a second crop of crystalline powder being collected by filtration.

$La\mathbf{L_{Ph}}(NO_3)_3$: Yield 70%. $C_{28}H_{26}LaN_7O_{11}$ (775.46): calcd. C 43.37, H 3.38, N 12.64; found C 43.37, H 3.43, N 12.42. IR (KBr): $\tilde{\nu}$ = 1610.27, 1571.70, 1494.56, 1463.71, 1428.99, 1294.00 cm^{-1}. MALDI-TOF MS: *m/z* (%) = 713 (100) $[La\mathbf{L_{Ph}}(NO_3)_2]^+$. ^1H NMR (400 MHz, [D$_3$]acetonitrile): δ = 1.26 (t, *J* = 7.15 Hz, 3 H) 2.27 (s, 1 H) 4.09 (d, *J* = 7.21 Hz, 2 H) 6.99 (d, *J* = 7.95 Hz, 1 H) 7.31–7.53 (m, 5 H) 7.80 (t, *J* = 8.01 Hz, 1 H) 8.19 (d, *J* = 7.82 Hz, 1 H) ppm. ^{13}C NMR (101 MHz, [D$_3$]acetonitrile): δ = 11.91, 48.94, 125.77, 128.42, 128.92, 130.23, 131.22, 140.92, 141.88, 151.57, 154.65, 163.45 ppm.

$Ce\mathbf{L_{Ph}}(NO_3)_3$: Yield 72%. $C_{28}H_{26}CeN_7O_{11}\cdot H_2O$: calcd. C 42.32, H 3.55, N 12.34; found C 42.85, H 3.24, N 12.41. MALDI-TOF MS: *m/z* (%) = 732 (100) $[Ce\mathbf{L_{Ph}}(NO_3)_2H_2O]^+$.

$Pr\mathbf{L_{Ph}}(NO_3)_3$: Yield 75%. $C_{28}H_{26}N_7O_{11}Pr$ (777.46): calcd. C 43.26, H 3.37, N 12.61; found C 43.19, H 3.08, N 12.57. IR (KBr): $\tilde{\nu}$ = 1608.34, 1583.27, 1571.70, 1494.56, 1463.71, 1428.99, 1419.35, 1297.86, 1282.43, 1263.15 cm^{-1}. MALDI-TOF MS: *m/z* (%) = 715 (100) $[Pr\mathbf{L_{Ph}}(NO_3)_2]^+$.

$Nd\mathbf{L_{Ph}}(NO_3)_3$: Yield 61%. $C_{28}H_{26}N_7NdO_{11}$ (780.79): calcd. C 43.07, H 3.36, N 12.56; found C 43.06, H 3.37, N 12.58. IR (KBr): $\tilde{\nu}$ = 1610.27, 1571.70, 1494.56, 1463.71, 1428.99, 1299.79, 1265.07 cm^{-1}. MALDI-TOF MS: *m/z* (%) = 718 (100) $[Nd\mathbf{L_{Ph}}(NO_3)_2]^+$.

$Sm\mathbf{L_{Ph}}(NO_3)_3$: Yield 61%. $C_{28}H_{26}N_7O_{11}Sm$ (786.95): calcd. C 42.74, H 3.33, N 12.46; found C 42.81, H 3.22, N 12.35. IR (KBr): $\tilde{\nu}$ = 1610.27, 1583.27, 1571.70, 1494.56, 1465.63, 1428.99, 1301.71, 1290.14 cm^{-1}. MALDI-TOF MS: *m/z* (%) = 726 (100) $[Sm\mathbf{L_{Ph}}(NO_3)_2]^+$.

$Eu\mathbf{L_{Ph}}(NO_3)_3$: Yield 65%. $C_{28}H_{26}EuN_7O_{11}$ (788.51): calcd. C 42.65, H 3.32, N 12.43; found C 42.81, 42.61; H 3.30, 3.34; N 12.27, 12.31. IR (KBr): $\tilde{\nu}$ = 1610.30, 1583.30, 1573.65, 1496.51, 1465.66, 1311.38, 1294.02, 761.76, 700.04, 674.97 cm^{-1}. MALDI-TOF MS: *m/z* (%) = 727 (100) $[Eu\mathbf{L_{Ph}}(NO_3)_2]^+$, 812 (13) $[Eu\mathbf{L_{Ph}}(NO_3)(PhCHCHCO_2H)]^+$, 449 (20) $[\mathbf{L_{Ph}} - H]^+$. ^1H NMR (400 MHz, [D$_3$]acetonitrile): δ = –0.27 (br. t, 3 H) 2.34 (br. s, 2 H) 3.42 (br. d, *J* = 7.34 Hz, 1 H) 3.64 (br. d, *J* = 7.83 Hz, 1 H) 5.29 (br. t, *J* = 7.58 Hz, 1 H) 7.39 (br. s, 5 H) ppm.

$Gd\mathbf{L_{Ph}}(NO_3)_3$: Yield: 70%. $C_{28}H_{26}N_7O_{11}Gd\cdot 2CH_3CN$ (875.90): calcd. C 43.88, H 3.68, N 14.39; found C 43.81, H 3.61, N 14.19. MALDI-TOF MS: *m/z* (%) = 732 (100) $[Gd\mathbf{L_{Ph}}(NO_3)_2]^+$.

$Tb\mathbf{L_{Ph}}(NO_3)_3$: Yield: 70%. MALDI-TOF MS: *m/z* (%) = 733 (30) $[Tb\mathbf{L_{Ph}}(NO_3)_2]^+$, 819 (100) $[Tb\mathbf{L_{Ph}}(NO_3)(PhCHCHCO_2)]^+$, 904 (100) $[Tb\mathbf{L_{Ph}}(PhCHCHCO_2)_2]^+$, 449 (15) $[\mathbf{L_{Ph}} - H]^+$.

$Dy\mathbf{L_{Ph}}(NO_3)_3$: Yield: 76%. $C_{28}H_{26}DyN_7O_{11}$ (799.05): calcd. C 42.09, H 3.28, N 12.27; found C 42.25, H 3.35, N 12.19. IR (KBr): $\tilde{\nu}$ = 1610.27, 1583.27, 1573.63, 1496.49, 1463.71, 1430.92, 1303.64, 1282.43 cm^{-1}. MALDI-TOF MS: *m/z* (%) = 738 (100) $[Dy\mathbf{L_{Ph}}(NO_3)_2]^+$.

$Ho\mathbf{L_{Ph}}(NO_3)_3$: Yield: 70%. $C_{28}H_{26}HoN_7O_{11}$ (801.48): calcd. C 41.96, H 3.27, N 12.23; found C 41.78, H 3.33, N 12.00. IR (KBr): $\tilde{\nu}$ = 1610.27, 1583.27, 1573.63, 1498.42, 1463.71, 1452.14, 1303.63, 1282.43 cm^{-1}. MALDI-TOF MS: *m/z* (%) = 739 (100) $[Ho\mathbf{L_{Ph}}(NO_3)_2]^+$.

$Er\mathbf{L_{Ph}}(NO_3)_3$: Yield: 62%. $C_{28}H_{26}ErN_7O_{11}$ (803.81): calcd. C 41.84, H 3.26, N 12.20; found C 41.82, H 3.27, N 12.01. IR (KBr): $\tilde{\nu}$ = 1610.27, 1583.27, 1571.70, 1496.49, 1463.71, 1452.14, 1305.57, 1282.43 cm^{-1}. MALDI-TOF MS: *m/z* (%) = 741 (100) $[Er\mathbf{L_{Ph}}(NO_3)_2]^+$.

$Tm\mathbf{L_{Ph}}(NO_3)_3$: Yield: 70%. $C_{28}H_{26}N_7O_{11}Tm$ (805.49): calcd. C 41.75, H 3.25, N 12.17; found C 41.82, H 3.27, N 12.24. IR (KBr): $\tilde{\nu}$ = 1612.28, 1583.35, 1573.71, 1496.56, 1465.71, 1452.21, 1430.99,

1384.71, 1288.28 cm^{-1}. MALDI-TOF MS: *m/z* (%) = 743 (100) $[TmL_{Ph}(NO_3)_2]^+$.

$YbL_{Ph}(NO_3)_3$: Yield: 87%. $C_{28}H_{26}N_7O_{11}Yb$ (809.59): calcd. C 41.54, H 3.24, N 12.11; found C 41.51, H 3.41, N 11.86. IR (KBr): $\tilde{\nu}$ = 1610.27, 1583.27, 1573.63, 1498.42, 1463.71, 1452.14, 1430.92, 1304.93, 1286.29 cm^{-1}. MALDI-TOF MS: *m/z* (%) = 748 (100) $[YbL_{Ph}(NO_3)_2]^+$.

$LuL_{Ph}(NO_3)_3$: Yield: 78%. $C_{28}H_{26}LuN_7O_{11}$ (811.52): calcd. C 41.44, H 3.23, N 12.08; found C 41.67, H 3.31, N 12.15. IR (KBr): $\tilde{\nu}$ = 1612.28, 1583.35, 1571.78, 1510.06, 1494.64, 1463.78, 1452.21, 1307.56, 1297.92, 1290.21 cm^{-1}. MALDI-TOF MS: *m/z* (%) = 749 (100) $[LuL_{Ph}(NO_3)_2]^+$. ^1H NMR (400 MHz, [D$_3$]acetonitrile): δ = 1.29 (t, *J* = 7.09 Hz, 3 H) 4.10 (q, *J* = 7.34 Hz, 2 H) 6.85 (d, *J* = 7.95 Hz, 1 H) 7.38–7.45 (m, 2 H) 7.48–7.58 (m, 3 H) 7.90 (t, *J* = 8.25 Hz, 1 H) 8.30 (d, *J* = 7.82 Hz, 1 H) ppm. ^{13}C NMR (151 MHz, [D$_3$]acetonitrile): δ = 11.81, 50.23, 126.14, 128.84, 130.98, 131.66, 141.46, 144.89, 149.80, 156.57, 173.78 ppm.

Supporting Information (see footnote on the first page of this article): NMR spectra (1D and 2D), atomic coordinates of minima on the PES (DFT), crystallographic data, atomic coordinates and molecule geometries from X-ray diffraction experiments, UV/Vis titrations.

Acknowledgments

This research is supported by the International Science and Technology Center (ISTC) (project N3364), Russian Foundation for Basic Research (RFBR) (projects 10-03-01163, 09-03-00603, 09-03-12065, 10-03-00898, and 13-03-01041), and the Ministry of Education and Science of the Russian Federation (program 14.513.11.0090). The Joint Supercomputer Center of the Russian Academy of Science (JSCC, Moscow) is acknowledged for the computing facilities. E. N. S. thanks the Basal Project FB 0807 for financial support. The NMR spectroscopic measurements were carried out in the Laboratory of Magnetic Tomography and Spectroscopy, Faculty of Fundamental Medicine, of Moscow State University.

[1] R. G. Watts, *Engineering Response to Global Climate Change: Planning a Research and Development Agenda*, 2nd ed., Taylor & Francis Group, **2013**.
[2] J. M. McKibben, *Radiochim. Acta* **1984**, *36*, 3.
[3] a) H. A. Abderrahim, D. De Bruyn, G. Van den Eynde, S. Michiels, *WIREs Energy Environ.* **2013**, 60–69; b) C. Zicari, C. Andenna, G. Felicioni, *J. Solid Waste Technol. Management* **2013**, *39*, 75–86.
[4] a) C. Hill, C. Madic, P. Baron, M. Ozawa, Y. Tanaka, *J. Alloys Compd.* **1998**, *271–273*, 159–162; b) G. Ionova, S. Ionov, C. Rabbe, C. Hill, C. Madic, R. Guillaumont, J. C. Krupa, *Solvent Extr. Ion Exch.* **2001**, *19*, 391–414; c) A. Bhattacharyya, P. K. Mohapatra, V. K. Manchanda, *Radiochim. Acta* **2010**, *98*, 141–147; d) B. Coupez, C. Boehme, G. Wipff, *J. Phys. Chem. B* **2003**, *107*, 9484–9490; e) D. R. Peterman, L. R. Martin, J. R. Klaehn, M. K. Harrup, M. R. Greenhalgh, T. A. Luther, *J. Radioanal. Nucl. Chem.* **2009**, *282*, 527–531.
[5] a) S. A. Ansari, P. N. Pathak, V. K. Manchanda, M. Husain, A. K. Prasad, V. S. Parmar, *Solvent Extr. Ion Exch.* **2005**, *23*, 463–479; b) S. Tachimori, Y. Sasaki, S.-i. Suzuki, *Solvent Extr. Ion Exch.* **2002**, *20*, 687–699; c) G. Modolo, H. Asp, C. Schreinemachers, H. Vijgen, *Solvent Extr. Ion Exch.* **2007**, *25*, 703–721; d) G. Modolo, H. Asp, H. Vijgen, R. Malmbeck, D. Magnusson, C. Sorel, *Solvent Extr. Ion Exch.* **2007**, *25*, 62–76.
[6] a) H. H. Dam, D. N. Reinhoudt, W. Verboom, *Chem. Soc. Rev.* **2007**, *36*, 367–377; b) M. Nilsson, S. Andersson, F. Drouet, C. Ekberg, M. Foreman, M. Hudson, J. O. Liljenzin, D. Magnusson, G. Skarnemark, *Solvent Extr. Ion Exch.* **2006**, *24*, 299–318; c) M. Nilsson, S. Andersson, C. Ekberg, M. R. S. Foreman, M. J. Hudson, G. Skarnemark, *Radiochim. Acta* **2006**, *94*, 103–106; d) M. Nilsson, C. Ekberg, M. Foreman, M. Hudson, J. O. Liljenzin, G. Modolo, G. Skarnemark, *Solvent Extr. Ion Exch.* **2006**, *24*, 823–843; e) M. J. Hudson, C. E. Boucher, D. Braekers, J. F. Desreux, M. G. B. Drew, M. R. S. J. Foreman, L. M. Harwood, C. Hill, C. Madic, F. Marken, T. G. A. Youngsa, *New J. Chem.* **2006**, *30*, 1171–1183; f) M. J. Hudson, L. M. Harwood, D. M. Laventine, F. W. Lewis, *Inorg. Chem.* **2013**, *52*, 3414–3428; g) D. M. Whittaker, T. L. Griffiths, M. Helliwell, A. N. Swinburne, L. S. Natrajan, F. W. Lewis, L. M. Harwood, S. A. Parry, C. A. Sharrad, *Inorg. Chem.* **2013**, *52*, 3429–3444.
[7] F. W. Lewis, L. M. Harwood, M. J. Hudson, P. Distler, J. John, K. Stamberg, A. Núñez, H. Galán, A. G. Espartero, *Eur. J. Org. Chem.* **2012**, 1509–1519.
[8] a) M. Alyapyshev, V. Babain, N. Borisova, I. Eliseev, D. Kirsanov, A. Kostin, A. Legin, M. Reshetova, Z. Smirnova, *Polyhedron* **2010**, *29*, 1998–2005; b) M. Y. Alyapyshev, V. A. Babain, N. E. Borisova, R. N. Kiseleva, D. V. Safronov, M. D. Reshetova, *Mendeleev Commun.* **2008**, *18*, 336–337.
[9] a) J. Yuan, G. Wang, *TrAC Trends Anal. Chem.* **2006**, *25*, 490–500; b) J.-C. G. Bünzli, C. Piguet, *Chem. Soc. Rev.* **2005**, *34*, 1048–1077; c) J.-C. G. Bünzli, *Chem. Rev.* **2010**, *110*, 2729–2755; d) J. C. G. Bünzli, in *Spectroscopic Properties of Rare Earths in Optical Materials*, vol. 83 (Eds.: R. Hull, J. Parisi, R. M. Osgood, Jr., H. Warlimont, G. Liu, B. Jacquier), Springer, Berlin, Heidelberg, **2005**, pp. 462–499.
[10] S. Shionoya, W. M. Yen, *Phosphor Handbook*, CRC Press Inc., Boca Raton, FL, 33431, USA, **1999**.
[11] J. Kido, Y. Okamoto, *Chem. Rev.* **2002**, *102*, 2357.
[12] a) K. Matsumoto, J. G. Yuan in *Metal Ions in Biological Systems, Vol. 40* (Eds.: A. Sigel, H. Sigel), Marcel Dekker Inc., New York, **2003**; b) J. Karvinen, V. Laitala, M.-L. Mäkinen, O. Mulari, J. Tamminen, J. Hermonen, P. Hurskainen, I. Hemmilä, *Anal. Chem.* **2004**, *76*, 1429–1436; c) J. Vuojola, M. Syrjänpää, U. Lamminmäki, T. Soukka, *Anal. Chem.* **2012**, *85*, 1367–1373; d) S. Mizukami, T. Yamamoto, A. Yoshimura, S. Watanabe, K. Kikuchi, *Angew. Chem. Int. Ed.* **2011**, *50*, 8750–8752; *Angew. Chem.* **2011**, *123*, 8909; e) J. Hovinen, P. M. Guy, *Bioconjugate Chem.* **2009**, *20*, 404–421; f) R. Badugu, J. R. Lakowicz, C. D. Geddes, *Bioorg. Med. Chem.* **2005**, *13*, 113–119; g) S. Mizukami, K. Tonai, M. Kaneko, K. Kikuchi, *J. Am. Chem. Soc.* **2008**, *130*, 14376–14377.
[13] a) E. Soini in *Rapid Methods and Automation in Microbiology and Immunology* (Ed.: K. O. Habermehl), Springer, Berlin, **1985**, pp. 414–421; b) K. Hanaoka, K. Kikuchi, S. Kobayashi, T. Nagano, *J. Am. Chem. Soc.* **2007**, *129*, 13502–13509; c) B. K. McMahon, T. Gunnlaugsson, *J. Am. Chem. Soc.* **2012**, *134*, 10725–10728; d) L. Albizu, M. Cottet, M. Kralikova, S. Stoev, R. Seyer, I. Brabet, T. Roux, H. Bazin, E. Bourrier, L. Lamarque, C. Breton, M.-L. Rives, A. Newman, J. Javitch, E. Trinquet, M. Manning, J.-P. Pin, B. Mouillac, T. Durroux, *Nat. Chem. Biol.* **2010**, *6*, 587–594.
[14] A. Bax, D. G. Davis, *J. Magn. Reson. (1969–1992)* **1985**, *63*, 207–213.
[15] a) B. P. Hay, J. R. Rustad, *J. Am. Chem. Soc.* **1994**, *116*, 6316–6326; b) B. P. Hay, D. Zhang, J. R. Rustad, *Inorg. Chem.* **1996**, *35*, 2650–2658; c) C. de Sahb, L. A. Watson, J. Nadas, B. P. Hay, *Inorg. Chem.* **2013**, *52*, 10632–10642.
[16] T. Le Borgne, J.-M. Bénech, S. Floquet, G. Bernardinelli, C. Aliprandini, P. Bettens, C. Piguet, *Dalton Trans.* **2003**, 3856–3868.
[17] F. Renaud, C. Piguet, G. Bernardinelli, J.-C. G. Bünzli, G. Hopfgartner, *Chem. Eur. J.* **1997**, *3*, 1646–1659.

[18] a) A. F. Kirby, D. Foster, F. S. Richardson, *Chem. Phys. Lett.* **1983**, *95*, 907; b) A. F. Kirby, F. S. Richardson, *J. Phys. Chem.* **1983**, *87*, 2544.
[19] L. N. Puntus, V. F. Zolin, *Russ. J. Coord. Chem.* **2003**, *29*, 574–581.
[20] N. Sabbatini, M. Guardigli, J.-M. Lehn, *Coord. Chem. Rev.* **1993**, *123*, 201.
[21] M. Kleinerman, *J. Chem. Phys.* **1969**, *51*, 2370.
[22] S. I. Klink, L. Grave, D. N. Reinhoudt, F. C. J. M. van Veggel, M. H. V. Werts, F. A. J. Geurts, J. W. Hofstraat, *J. Phys. Chem. A* **2000**, *104*, 5457.
[23] A. J. Bard, R. Parsons, J. Jordan, *Standard Potentials in Aqueous Solution*, Marcel Dekker Inc., New York, **1985**.
[24] a) L. N. Puntus, V. F. Zolin, V. A. Kudryashova, V. A. Tsaryuk, J. Legendziewicz, P. Gawryszewska, R. Szostak, *Phys. Solid State* **2002**, *44*, 1440–1444; b) V. F. Zolin, L. N. Puntus, V. I. Tsaryuk, V. A. Kudryashova, J. Legendziewicz, P. Gawryszewska, R. Szostak, *J. Alloys Compd.* **2004**, *380*, 279–284.
[25] V. Tsaryuk, V. Zolin, L. Puntus, V. Savchenko, J. Legendziewicz, J. Sokolnicki, R. Szostak, *J. Alloys Compd.* **2000**, *300–301*, 184–192.
[26] R. Demirbilek, J. Heber, S. I. Nikitin, *Proc. SPIE* **2002**, *4766*, 47–50.
[27] C. K. Jörgensen, *Mol. Phys.* **1962**, *5*, 271.
[28] M. Latva, H. Takalo, V.-M. Mukkala, C. Matachescu, J. C. Rodríguez-Ubis, J. Kankare, *J. Lumin.* **1997**, *75*, 149–169.
[29] M. H. V. Werts, R. T. F. Jukes, J. W. Verhoeven, *Phys. Chem. Chem. Phys.* **2002**, *4*, 1542–1548.
[30] *Saint*, version 8.27A, Bruker AXS Inc., Madison, Wisconsin, USA, **1997–2012**.
[31] R. H. Blessing, *Acta Crystallogr.* **1995**, *A51*, 33–38.
[32] G. M. Sheldrick, *Acta Crystallogr.* **2008**, *A64*, 112–122.
[33] a) D. Laikov, Y. Ustynyuk, *Russ. Chem. Bull. Int. Ed.* **2005**, *54*, 820–826; b) D. N. Laikov, *Chem. Phys. Lett.* **1997**, *281*, 151–156.
[34] a) J. P. Perdew, K. Burke, M. Ernzerhof, *Phys. Rev. Lett.* **1996**, *77*, 3865; b) J. P. Perdew, K. Burke, M. Ernzerhof, *Phys. Rev. Lett.* **1997**, *78*, 1396.
[35] a) W. J. Stevens, H. Basch, M. Krauss, *J. Chem. Phys.* **1984**, *81*, 6026–6033; b) W. J. Stevens, M. Krauss, H. Basch, P. G. Jasien, *Can. J. Chem.* **1992**, *70*, 612–630.
[36] R. G. Dyall, *J. Chem. Phys.* **1994**, *100*, 2118–2127.
[37] D. N. Laikov, *Chem. Phys. Lett.* **2005**, *416*, 116–120.
[38] P. M. Polestshuk, T. V. Magdesieva, *Inorg. Chem.* **2010**, *49*, 3370–3386.

Received: September 29, 2013
Published Online: March 21, 2014

